fluids

MDPI

Review

Updated Review on the Available Methods for Measurement and Prediction of the Mass Transfer Coefficients in Bubble Columns

Stoyan Nedeltchev

Institute of Chemical Engineering, Polish Academy of Sciences, 5 Baltycka Str., 44-100 Gliwice, Poland; sned@iich.gliwice.pl

Abstract: This review summarizes the most important measurement techniques for determination of the volumetric liquid-phase mass transfer coefficient k_La. In addition, the main empirical correlations (with their applicability ranges) for k_La estimation are presented. It is clearly underlined that in tall bubble columns, a system of two differential equations (involving the gas and liquid axial dispersion coefficients) should be solved in order to obtain the accurate k_La value. The semi-empirical correlations for k_La prediction based on the correction of the penetration theory are also summarized. The need for a correction of the penetration theory is explained. The different definitions of the gas–liquid contact time, including the one based on the local isotropic turbulence theory, are presented. Finally, the various chemical methods for the determination of the gas–liquid interfacial area are summarized. Additionally, the main correlation for the prediction of the interfacial area is reported. The effects of pressure, temperature, and viscosity on the interfacial area and k_La are discussed.

Keywords: bubble columns; mass transfer coefficient; empirical correlations; penetration theory; correction factor; local isotropic turbulence theory

check for updates

Academic Editor: T. Hoehne

Received: 16 December 2024
Revised: 14 January 2025
Accepted: 22 January 2025
Published: 27 January 2025

Citation: Nedeltchev, S. Updated Review on the Available Methods for Measurement and Prediction of the Mass Transfer Coefficients in Bubble Columns. *Fluids* **2025**, *10*, 29. https://doi.org/10.3390/fluids10020029

Copyright: © 2025 by the author. Licensee MDPI, Basel, Switzerland. This article is an open access article distributed under the terms and conditions of the Creative Commons Attribution (CC BY) license (https://creativecommons.org/licenses/by/4.0/).

1. Introduction

Bubble columns (BCs) are widely used in chemical, biochemical, biotechnological, and petrochemical industries mainly due to their simple design (no moving parts) and operation, as well as excellent heat transfer and mass transfer (MT) properties. In these gas-liquid contactors the MT rate between a gas and liquid is limited by the diffusion of the solute in the liquid. The simple construction of BCs causes complex hydrodynamic and MT properties since no installments provide for repeated redistribution of gas and liquid and no additional mechanical energy is introduced to the gas–liquid dispersion [1]. BCs are characterized with a large interfacial area per unit dispersion volume and intense liquid agitation, which enhances the mixing of solutes and accelerates chemical reactions.

BCs are very suitable units for performing aerobic fermentation processes. High oxygen transfer efficiencies can be obtained in tall BCs. The variables deserving special consideration are the size and shape of the bubbles; their rise velocity, circulation, and coalescence; effects of surface-active substances; and the MT rate. The latter depends on the hydrodynamics near the interface. For a rough estimation of the MT efficiency, the volumetric liquid-phase mass transfer coefficient k_La is usually applied. Bubble volume and bubble shape determine the surface-to-volume ratio, which is a very important parameter in estimating the overall MT rates. It is essential in the scale-up and design of BCs to be able to predict the MT rates reliably. The MT properties of the bubbles in liquids determine the efficiency and dimensions of BCs. Since the size, shape, and velocity of the bubble

may change appreciably as it rises and dissolves, its MT coefficient may vary accordingly. Enhancing gas–liquid MT in industrial applications could effectively reduce the equipment size, improve productivity, and reduce operating and production costs, thereby realizing low-energy and high-efficiency production.

Irrespective of the simple BC construction, there is a complex interaction and mixing of the phases. The successful scale-up of BCs requires a deep understanding of the MT efficiency. The gas–liquid MT is one of the key factors for BC performance. It is strongly affected by the hydrodynamics, phase mixing, and physical properties.

In tall BCs, the bubble size variation is essentially controlled by both MT and pressure effects. In these facilities, the bubble diameter in the lower zone of the column becomes smaller due to the high MT flux, whereas it increases slightly in the upper zone due to the volume expansion caused by the reduced hydrostatic head. Tall BCs are advantageous for MT due to the increased gas residence time and gas solubility [1].

Owing to their excellent MT and heat transfer characteristics as well as low operational costs, these gas–liquid contactors are frequently used in chemical processes such as absorption (with and without chemical reaction), oxidation, chlorination, alkylation, polymerization and hydrogenation, etc. Complex flow patterns (structures) are formed in BCs, and they affect both liquid mixing and MT. According to Deckwer and Schumpe [2], BCs are particularly well suited for gas–liquid reactions taking place in a slow reaction-absorption regime. In addition, these gas–liquid contactors are used in the biochemical process of fermentation and biological wastewater treatment. The discontinuous gas phase is dispersed in the continuous liquid phase through a gas distributor (perforated plate, porous plate, cross sparger, single tube, etc.), which should be well designed in order to avoid gas maldistribution.

The MT limitations are one of the main bottlenecks in many chemical processes. Usually, the MT rate is determined by several important parameters such as the liquid-phase MT coefficient k_L, the gas–liquid interfacial area a, and the saturation concentration of the dissolved gas. In the case of bubble beds with short and medium heights, the saturation concentration is constant in the axial direction. The liquid-phase MT coefficient k_L quantifies the rate of substance transfer between gas and liquid phases per unit area per concentration difference, which is crucial for the process efficiency. When the solubility of the gaseous compound in the solution increases, this improves the MT of chemical reactions. It is worth noting that the smaller the bubble, the greater the gas solubility. Several limitations (mixing, viscosity, etc.) affect the MT effectiveness. When the viscosity is increased, it imposes a substantial constraint on MT.

The generated flow patterns inside the BC are quite complex, and they affect the mixing, MT, and heat transfer. The gas sparger design significantly affects the hydrodynamics and the gas holdup only in the bubbly flow regime. In the churn-turbulent flow regime, the sparger design has an effect only in the entrance region [3,4]. In the case of gas absorption, the bubble shrinkage in the lower zone of the BC leads to enhanced MT. The bubble shrinkage leads to significant bubble aspect ratio changes. In tall BCs, due to the reduced hydrostatic head, the bubbles expand in the upper zone of the BC [1]. Usually, the bubbles reach a minimum stable size of 1 mm and then do not shrink further. The MT from the bubbles into the liquid does not only depend on the initial bubble size but also on the mode of operation (co-current or counter-current). The MT from the bubbles to the liquid changes the bubble size and shape during the bubble rise. The enhancement of the liquid-phase turbulence (by selecting the proper operational mode) could be beneficial for both gas–liquid mixing and MT.

For a successful BC design, a good understanding of the interactions between both phases is essential. This includes knowledge of both hydrodynamic (bubble size and shapes, gas fraction and rise velocities) and MT (interfacial area and volumetric liquid-phase MT coefficient $k_L a$) characteristics. The gas–liquid interfacial area could be measured

by means of a four-point optical probe [5]. This method is especially advantageous in opaque BCs. The fluid dynamics of the rising gas bubbles have been extensively studied. However, the majority of case studies have been focused on the air–water system. A phenomenological understanding of the interplay between hydrodynamics and MT is essential for the development of improved MT models.

Important Findings About the MT Process in BCs

Deckwer et al. [6] have demonstrated the large influence of the gas sparger on the k_L. The main MT correlations by 1980 have been tabulated in [6]. It is underlined that the predictions from the different MT correlations differ substantially. As main reasons for these deviations, Deckwer et al. [6] have indicated the application of inappropriate measurement techniques and evaluation of the k_L value by means of oversimplified model assumptions. The main MT correlations lead to appreciably different predictions as none of them explicitly consider the gas sparger characteristics. The gas sparger effect becomes negligible at high superficial gas velocities U_g and in tall BCs. In short BCs, the k_La value significantly depends on the liquid height.

In many cases, the single-point liquid concentration measurements are not enough to obtain reliable MT coefficients. In addition, pertinent MT models should be used in order to obtain a reliable database of MT coefficients. In the case of physical absorption of carbon dioxide in water, only when increased k_L value was applied in the region adjacent to the gas sparger was a satisfactory description of the experimental liquid-phase concentrations in the lower zone of the column achieved. Deckwer et al. [6] found that the k_L value used to match the measured liquid concentration profiles did not depend only on the type of the gas sparger but also on the selection of absorption or desorption processes or co-current or counter-current modes of operation. One of the authors' hypotheses is that the increased k_L value at the column bottom is most likely caused by the enhanced turbulence intensity due to the high energy dissipation rate in the vicinity of the gas sparger.

In the case of physical absorption of carbon dioxide in water, Deckwer et al. [6] argue that the U_g value is variable, and as a result of that, both the interfacial area and gas holdup vary with the axial position. The authors concluded that if the gas sparger zone is separated from the rest of the bubble bed, then the experimental MT data could be fitted with a constant k_L value along the column. In the case of oxygen MT studies in tall BCs, it was found [6] that sintered plates yield appreciably higher k_L values than perforated plates with orifices larger than 0.5 mm.

When physical absorption is investigated, opposite effects of gas shrinkage (in the lower zone of the column) and gas expansion (in the upper zone) are observed due to the reduced hydrostatic head [7]. Deckwer [7] argues that the neglect of the variable U_g may yield serious errors even under isobaric conditions. The MT from gas to liquid phase can considerably decrease the gas volume. The MT can be enhanced by the reaction in the liquid phase.

Deckwer [7] reported that in the case of concurrent flow, both the dimensionless gas velocity and concentration run through a minimum when they are plotted against the dimensionless axial coordiate. The minimum in the dimensionless gas concentration corresponds to a maximum in the dimensionless liquid concentration. The reason for that is the equilibrium between absorption and desorption. The author argues that in the vicinity of the gas distributor, the highest absorption rate is observed, since the driving concentration difference is the highest due to the pure entering liquid and the hydrostatic head. This is the reason for the decrease in the U_g value. In the axial direction, the MT rate decreases and cannot compensate for the gas expansion due to the reduced hydrostatic head. Due to this reason, Deckwer [7] argues that the U_g value increases in the axial direction as the gas holdup is kept constant. Near the bottom of the column, the liquid becomes supersaturated with regards to

the pressure at the column's top; thus, in the upper zone of the column, desorption occurs. If the reaction rate in the liquid phase is fast enough, desorption is not observed, and the minimum disappears. Deckwer [7] has found that the oxygen uptake increases with the decrease of the column diameter.

Deckwer et al. [1] argue that simpler MT models can be applied only if the column operates at elevated pressures and if the gas shrinkage due to absorption is small. Operating conditions corresponding to high carbon dioxide solubility lead to large interphase MT flow rates. It is noteworthy that the available MT correlations cannot be reliably applied to operating conditions, which correspond to high interphase MT rates. According to Deckwer et al. [1], both MT and pressure drop are responsible for the variations of the gas volume flow rate, which affects the main fluid dynamic properties.

In the case of no appreciable MT and in short BCs, Deckwer et al. [1] argue that the gas holdup does not vary in the axial direction. In tall BCs, the local gas holdup increases with column length due to volume expansion caused by decreasing hydrostatic pressure. A very important finding is that, in the case of desorption, the dependence of gas holdup on the axial position is more pronounced. The reason is that both pressure drop and MT increase the gas holdup. Since the bubble diameter depends on the turbulence within the dispersion, the interfacial area also depends on the turbulence and thus the $k_L a$ value. Deckwer et al. [1]. argue that the MT resistance is limited to the liquid side. When no chemical reaction takes place in the gas phase and the gas concentrations are rather high, gas-side resistances do not occur.

The carbon dioxide concentration profiles could be determined by both electrochemical and/or titration methods. Deckwer et al. [1] argue that enhanced MT occurs in the region adjacent to the gas sparger. In this zone, the flow pattern is not uniform since strong turbulence occurs. At a length of 0.5–1.0 m, a quasi-homogeneous gas–liquid dispersion is formed, which flows rather uniformly towards the top of the column. The authors argue that the MT coefficients decrease with the increase of the bubble densities.

Nedeltchev et al. [8] have reported radial $k_L a$ profiles at four axial positions and at three different U_g values in the case of physical absorption of carbon dioxide into water. Additional discussion of MT in BCs can be found in the following articles: Martin et al. [9], Xu et al. [10], Miguet et al. [11], Hu et al. [12], Dong et al. [13], and Hebrard et al. [14].

2. Measurement Techniques and Methods for $k_L a$ Estimation

The gas–liquid MT plays a key role for the BC performance. Numerous articles devoted to gas–liquid MT in BCs have been published in the past five decades. In most of the articles, the MT performance of BCs is estimated in terms of the volumetric liquid-side MT coefficient $k_L a$. The latter is a global result of two contributions: the resistance to MT in the liquid phase and the gas–liquid interfacial area. The MT time is inversely proportional to the $k_L a$ coefficient. In a batch BC without chemical reaction, the MT time determines the operational time of the reactor. However, the MT process can be enhanced by means of a chemical reaction and liquid turbulent eddies.

The modern methods for the measurement of the MT coefficient are summarized in Table 1.

Table 1. Summary of the modern methods for MT measurements.

Measurement Technique	Reference	Model
Oxygen optode	Terasaka et al. [15]	Complete mixing
Oxygen-enriched air dynamic method, optical O_2 probe	Han and Al-Dahhan [16]	ADM for both phases
Laser-induced fluorescence (LIF) technique by means of a pH-sensitive dye	Huang and Saito [17] Valiorgue et al. [18]	Complete mixing

The driving force for gas–liquid MT is usually a result of the dynamic change of gas or liquid input (pulse or step), by pressurizing the gas step or by the presence of chemical reactions [16]. MT needs certain time in order to attain a steady state. The dynamic gas absorption or desorption method has been frequently used in BCs due to its simplicity and reliability. The method is applied by means of switching the gas flow between air and nitrogen. Han and Al-Dahhan [16] have created an oxygen-enriched air dynamic method to overcome the differences associated with all the previous methods. While maintaining the main air flow, a small oxygen flow is added to achieve the switch between air and oxygen-enriched air. In the dynamic method, the measured transient concentration profiles of the introduced gas represent not only the degree of the gas–liquid MT but also the phase mixing. Hence, an accurate reactor model is needed to estimate the k_La values by fitting the recorded data.

By means of the optical oxygen probe (a fluorescence-type sensor), the dissolved oxygen (DO) concentration is measured in the bubble bed. This sensor is characterized with a fast response, stability, and long life [16]. A thin film coated on the probe tip emits fluorescence at about 600 nm (when irradiated at 475 nm) by means of the light source. The increase of the DO concentration quenches the 600 nm fluorescence linearly. The DO concentrations are obtained by measuring the fluorescence intensity by means of spectrometer. Han and Al-Dahhan [16] have explained in detail that there is always a delay in the sensor response and how it should be taken into account. The optical probe constant is usually estimated by means of a calibration process.

Han and Al-Dahhan [16] have shown how the k_La value can be determined by both complete mixing model and axial dispersion model (ADM). The authors argue that the one-dimensional ADM should be solved for both liquid and gas phases. In such a way, the k_La value can be obtained as a fitted parameter. The authors have assumed that the local gas holdup is equal to the overall gas holdup, which was measured be means of the observation of the bed expansion. Han and Al-Dahhan [16] have found that the gas sparger has a noticeable effect on the k_La at U_g values lower than 0.15 m/s. There is only a slight effect in the high U_g range beyond 0.2 m/s. As the operating pressure was elevated, k_La values increased due to the bubble shrinkage. The effect of the gas sparger on the k_La values has not been studied well.

Han and Al-Dahhan [16] have shown that there are differences in the k_La estimation when the assumption of perfect mixing and the ADM are being compared. The differences are more pronounced in the upper zone of the column. The authors have reported that the k_La value in the case of the complete mixing assumption is about 30% lower. Han and Al-Dahhan [16] have also investigated the effect of the orifice diameter of the perforated plate spargers on the k_La values. The authors argue that the orifice diameters affect both the bubble size and interfacial area in the entire bubble bed. Han and Al-Dahhan [16] have found that the U_g value should be higher than the main transitional velocity in order to satisfactorily eliminate the sparger's effect on the k_La values. At high U_g values, both the hydrodynamics and phase mixing are similar irrespective of the gas sparger type. The bubble sizes are also similar. The k_La values increase with the increase of U_g and the operating pressure. The interfacial area increases greatly due to the smaller bubble size generated at high pressure [19,20].

Oxygen is dissolved in the liquid phase due to a concentration gradient that exists between the bubbles and the bulk solution. The bubble diameter is the key parameter in the MT calculations. It affects the bubble rise velocity, MT coefficient, and surface area. It should be taken into account that the bulk liquid concentration changes over time, and the bubble size changes as it rises through the column. Usually, the probe constant is about one magnitude larger than the k_La value, which implies that the time scale for the probe delay is small enough for k_La measurements.

In the case of gas absorption, the effect of bubble shrinkage (in the lower zone of the column) on both the hydrodynamics and MT are not well studied. The bubble size and shape along with the liquid properties play a key role in the estimation of the MT coefficient. The bubble shape (spherical, ellipsoidal, wobbly, or spherical-cap) affects the gas–liquid interfacial area available for interfacial MT.

One of the latest experimental approaches for measuring the dissolved CO_2 concentration is to apply the laser-induced fluorescence (LIF) technique by means of a pH-sensitive dye [18]. A moving high-speed camera system is used. One of the main advantages of this technique is the visualization of the instantaneous MT in the wake of a bubble. This contribution to MT will be extensively studied in the next decade.

In the case of rigid spherical bubbles, the classical penetration model put forward by Higbie [21] can be used successfully for the prediction of the liquid-phase MT coefficients k_L. This MT model takes into account the interfacial mobility and the influence of the liquid flow around the bubble. Higbie's model [21] is defined based on the concept of a constant gas–liquid exposure time for an axisymmetric flow around a spherical bubble. The contact (exposure) time is usually expressed as the ratio of the mean bubble size to the bubble rise velocity. The local bubble size, gas volume fraction and average vertical bubble velocity could be measured by means of a dual-tip optical fiber probe. The contact time couples the bubble size and its motion to the gas–liquid interfacial area available for MT. It is noteworthy that Higbie's penetration model [21] does not include the bubble shape and wake effects on the MT. In addition, the bubble shape oscillations when the bubbles rise are also not considered in the penetration model. A better understanding of the effect of the bubble hydrodynamics on the MT process is required. Several researchers have studied how this correlation changes in both pure and contaminated liquids. It was found that this theory is applicable to operating conditions involving small bubble sizes (lower than 3.0 mm). In the case of larger bubbles, a correction factor should be applied [22,23]. For the simple case of a shrinking CO_2 bubble rising in water, it has been observed that at smaller bubble sizes (less than 2.0 mm), the prediction of the k_L coefficient should be based on the correlation for the immobile interface, whereas for bubble diameters between 2.0 and 3.0 mm, the k_L predictions fall within the boundaries of the correlations for mobile and immobile interfaces [24,25]. This result could be attributed to the presence of a small amount of contaminant, which affects to a different extent both the smaller and bigger bubbles. The authors argue that the observed shape oscillations in larger bubbles repel the contamination layer, rendering them mobile.

The different approaches for estimating the gas holdups, mixing, and MT coefficients have been reviewed exhaustively in Deckwer and Schumpe [2] and Leonard et al. [26]. The main disadvantage of BCs is their considerable backmixing in both phases, high pressure drop, and bubble coalescence. One of the main goals is to suppress the backmixing in order to improve the MT performance. The effect of the elevated pressure and bed aspect ratio on k_La has been studied by Letzel et al. [27], Maalej et al. [28], Jordan and Schumpe [29,30], Lin et al. [19], Lau et al. [31] and Gopal and Sharma [32].

3. Empirical MT Correlations

3.1. Correlation of Akita and Yoshida [33]

The correlation proposed by Akita and Yoshida [33] is considered one of the most reliable at ambient pressure:

$$\frac{k_L a D_C^2}{D_L} = 0.6\left(\frac{\mu_L}{\rho_L D_L}\right)^{0.5}\left(\frac{g D_C^2 \rho_L}{\sigma_L}\right)^{0.62}\left(\frac{g D_C^3 \rho_L^2}{\mu_L}\right)^{0.31}\varepsilon_g^{1.1} \quad (1)$$

Various gas–liquid systems (air, O_2, CO_2, He/water, glycol solutions, glyecerol solutions, methanol and 0.15 M sodium sulfite solution) have been used. This equation has been proven to be applicable for scale-up [2], especially for an air/CO_2/water system. Most of the operating conditions cover oblate ellipsoidal bubbles.

3.2. Correlation of Hikita et al. [34]

Another dimensionless correlation that is valid for both electrolyte and non-electrolyte solutions has been proposed by Hikita et al. [34]. The authors have used four different gases (O_2, H_2, CO_2 and CH_4) and have considered the gas viscosity:

$$\frac{k_L a U_g}{g} = 14.9 f \left(\frac{U_g \mu_L}{\sigma_L} \right)^{1.76} \left(\frac{g \mu_L^4}{\rho_L \sigma_L^3} \right)^{-0.248} \left(\frac{\mu_G}{\mu_L} \right)^{0.243} \left(\frac{\mu_L}{\rho_L D_L} \right)^{-0.604} \quad (2)$$

where $f = 1$ for non-electrolytes (water, 1-butanol, methanol and sugar solutions), and f is a function of ionic strength when electrolyte solutions are being used. Most of the operating conditions cover oblate ellipsoidal bubbles.

3.3. Correlation of Jordan and Schumpe [29]

Jordan and Schumpe [29] have developed a reliable correlation for prediction of the $k_L a$ values in various organic liquids (ethanol (96%), 1-butanol, toluene, and decalin) aerated with different gases (nitrogen and helium) not only at ambient pressure but also at elevated pressures. The BC (0.1 m in ID) was equipped with three different types of perforated plates (19 × ∅ 1.0 mm; 1 × ∅ 1.0 mm; and 1 × ∅ 4.3 mm). The BC was operated at head pressures up to 4.0 MPa. Jordan and Schumpe [29] have reported various $k_L a$ values obtained in different organic liquids. The dimensionless MT correlation reads as follows:

$$Sh = a Sc^{0.5} Bo^{0.34} Ga^{0.27} Fr^{0.72} \left(1 + 13.2 Fr^{0.37} \left(\frac{\rho_G}{\rho_L} \right)^{0.49} \right) \quad (3)$$

The definitions of the dimensionless numbers could be found in the original article [29]. It is worth noting that the authors used a constant bubble diameter of 3 mm in their correlation. The dimensionless numbers were varied in the following ranges: $71 \leq Sc \leq 68.9 \times 10^3$, $1.21 \leq Bo \leq 5.39$, $825 \leq Ga \leq 1.55 \times 10^6$, $0.06 \leq Fr \leq 1.22$. Most of the operating conditions cover oblate ellipsoidal bubbles.

It is noteworthy that a distinction between $k_L a$ values referring to dispersion volume and $k_L a$ values referring to liquid volume has been only made in the articles of Prof. Schumpe. In the MT measurements of Jordan and Schumpe [29], the oxygen desorption from the liquid was traced with an optical probe based on fluorescence extinction by oxygen. The fluorophore was dissolved in the liquid, and in such a way, an instantaneous response was achieved.

The schematic of the experimental setup used by Jordan and Schumpe [29] is shown in Figure 1. The gas was always passing through a saturator filled with the same organic liquid before entering the BC. This is the correct way of performing MT measurements in BCs operated with organic liquids.

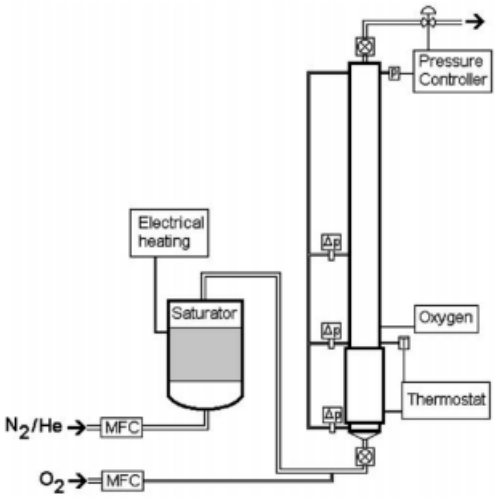


Figure 1. Schematic of the BC facility used by Jordan and Schumpe [29].

3.4. Correlation of Öztürk et al. [35]

These authors have also developed an MT correlation that is explicitly valid for organic liquids at ambient pressure:

$$\frac{k_L a d_B^2}{D_L} = 0.62\left(\frac{\mu_L}{\rho_L D_L}\right)^{0.5}\left(\frac{g d_B^2 \rho_L}{\sigma_L}\right)^{0.33}\left(\frac{g d_B^3 \rho_L^2}{{\mu_L}^2}\right)^{0.29}\left(\frac{U_g}{\sqrt{g d_B}}\right)^{0.68}\left(\frac{\rho_G}{\rho_L}\right)^{0.04} \quad (4)$$

The researchers argue that for the development of Equation (4), over 400 $k_L a$ values in 50 different gas–liquid systems in a relatively narrow BC (0.095 m in ID) have been measured. Deckwer and Schumpe [2] recommend a constant bubble diameter equal to 3 mm be considered in Equation (4). However, this assumption is questionable. The dimensionless numbers were varied in the following ranges: $32 \leq Sc \leq 1.5 \times 10^5$, $1.2 \leq Bo \leq 5.4$, $830 \leq Ga \leq 1.50 \times 10^6$, $4.3 \times 10^{-2} \leq Fr \leq 6.0 \times 10^{-1}$ and $16 \leq Sc \leq 970$. Most of the operating conditions cover oblate ellipsoidal bubbles.

Some additional correlations have been summarized in Deckwer and Schumpe [2]. They are valid for the cases of viscous Newtonian and non-Newtonian media, which are frequently used in both biotechnology and polymer processing.

3.5. Empirical MT Correlation for Two-Phase and Three-Phase BCs [36]

Lemoine et al. [36] have developed an alternative MT correlation, which is valid for both two-phase and three-phase BCs. According to this correlation, the $k_L a$ values depend on the Sauter-mean bubble diameter d_S. The latter should be calculated according to the correlation of Lemoine et al. [36]. Except for the physicochemical properties and the superficial gas velocity, the d_S correlation depends on the concentration of the purest component in the liquid mixture, volumetric solid concentration, and diameter and density of the solid particles. In two-phase BCs, the last three parameters should be considered equal to zero and eliminated from the d_S correlation. Lemoine et al. [36] have proposed the following MT correlation:

$$k_L a = 6.14 \times 10^4 \frac{{\rho_L}^{0.26}{\mu_L}^{0.12}}{{\sigma_L}^{0.52}{\rho_G}^{0.06}} \frac{{\varepsilon_g}^{1.21}}{{U_g}^{0.12}{d_S}^{0.05}} \frac{{D_L}^{0.5}}{T^{0.68}} G^{0.11}\left(\frac{D_C}{D_C + 1}\right)^{0.4} \quad (5)$$

G is a parameter that characterizes the gas sparger type. The range of applicability of Equation (5) is specified in Lemoine et al. [36]. Most of the operating conditions cover oblate ellipsoidal bubbles.

4. Semi-Theoretical Approaches for k_La Prediction Based on the Penetration Theory [21]

4.1. Correction Factor Proposed by Miller [22]

Miller [22] has demonstrated that MT depends on the mean bubble diameter. The MT in the BC is controlled by the MT around a single bubble in fluid at rest. The liquid agitation plays a minor role in the MT at the bubble interface. Bubble shape, motion, and the frequency extent of interface fluctuations also affect the MT coefficient. The change in the bubble shape affects not only the interfacial area but also the liquid-phase MT coefficient k_L. Bubbles moving in low-viscosity liquids are first distorted to oblate ellipsoidal shape. Usually, the bubble shape is characterized in terms of the bubble eccentricity. According to Miller [22], the prediction of the k_L value by means of Higbie's penetration theory [21] should be multiplied by a correction factor f_c, which is a single function of the bubble size: $f_c = 683{d_B}^{1.376}$. Originally, this correction factor f_c was developed for the stripping of CO_2 from aqueous solution with air.

Since the MT coefficient depends on the bubble shape, the addition of surface-active agents causes a decrease in bubble distortion. As the liquid viscosity increases, the bubble deformation reduces [37]. On the other hand, Calderbank [38] found a decrease in the eccentricity (maximum width to maximum height) with increasing viscosity. The process was accompanied by the appearance of "tails" behind small bubbles and of spherical indentations in the rear surfaces.

4.2. Correction Factor Proposed by Nedeltchev et al. [23]

In the case of non-spherical bubbles, the group of Prof. Nedeltchev [23] argue that Higbie's penetration theory [21] cannot be applied directly, and some correction factor f_c (lower than unity) should be introduced. It has been demonstrated that it is a function of the Eötvös number *Eo* and a dimensionless gas density ratio: $f_c = 0.124Eo^{0.94}$(dimensionless density ratio)$^{0.15}$. Overall, 263 experimental k_La values have been fitted with the new correction factor. The BCs (0.1 m and 0.095 m in ID) have been equipped with four different gas spargers (19 × ∅ 1.0 mm; 1 × ∅ 4.3 mm; 1 × ∅ 1.0 mm; and single tube ∅ 3.0 mm). Not only air but also nitrogen and helium have been used. The authors [23] argue that this factor combined the individual corrections of both the liquid-phase mass transfer coefficient k_L and the gas–liquid interfacial area. The introduction of the dimensionless density ratio was needed since the correlation for the bubble size was tested only up to 1.5 MPa. In the work of Nedeltchev et al. [23], k_La values up to 4.0 MPa have been used, which could not be fitted without this additional term. In this approach, the gas–liquid contact time (needed for the k_L calculation) has been defined as a ratio of the bubble surface to the rate of surface formation. Both parameters depend predominantly on the geometrical characteristics (length and height) of the ellipsoidal bubbles. They are functions of both the mean bubble diameter and Tadaki number. It was found that, by means of the new correction factor, the experimental k_La values could be predicted reasonably well.

The following organic liquids have been studied: acetone, anilin, benzene, 1-butanol, cyclohexane, decalin, ethanol, ethyl acetate, ethylbenzene, 1,2-dichloroethane, 1,4-dioxane, ligroin, methanol, nitrobenzene, 2-propanol, tetralin, toluene, and xylene. In addition, two mixtures (benzene/cyclohexane and toluene/ethanol) in different concentrations have been investigated. The new correction factor also predicts well the k_La values in tap water.

4.3. Contact Time Defined by Means of the Local Isotropic Turbulence Theory [39]

Deckwer [39] argues that the gas–liquid contact time characterizes the residence time of microeddies at the interface. According to local isotropic turbulence theory, the large primary eddies contribute, to a minor extent, to a viscous energy dissipation in the bubble

bed. However, the motion of the large eddies generates small eddies, which dissipate the energy by means of viscous forces. In case of high Reynolds number, the energy dissipation by the micro-scale eddies becomes locally isotropic. In such a way, the gas–liquid contact time can be defined on the basis of only the kinematic viscosity and the energy dissipation rate per unit mass. It is defined as the ratio of the length scale η (see Equation (6)) to velocity scale υ (see Equation (7)) of the micro eddies. Both parameters can be expressed as follows:

$$\eta = \left(\frac{\nu^3}{\in}\right)^{0.25} \tag{6}$$

$$\upsilon = (\nu \in)^{0.25} \tag{7}$$

The energy dissipation rate per unit mass is usually expressed as a product of both g and superficial gas velocity U_g. Based on this definition of the gas–liquid contact time, it could be further applied to Higbie's penetration theory [21]. It has been shown that turbulent eddies can enhance the MT by causing the renewal of the liquid close to the interface.

In Table 2 are summarized all MT approaches based on the classical penetration theory.

Table 2. Summary of the approaches based on the correction of Higbie's theory.

Correction Factor	Reference	Contact Time
Single function of bubble size	Miller [22]	Bubble diameter/rise velocity
Function of *Eo* number	Nedeltchev et al. [23]	Bubble surface/rate of surface formation
No correction	Deckwer [39]	Length scale/velocity scale of microeddies

5. Computational Methods for Estimation of the Liquid-Phase MT Coefficients

In the past two decades, many new approaches for prediction of the MT coefficients based on computational fluid dynamics (CFD) have been developed. The following articles could be recommended: Li et al. [40], Chen and Brooks [41], Hissanaga et al. [42], Liu et al. [43], Rzehak and Krepper [44], Jain et al. [45], Krauß and Rzehak [46], Jia and Zhang [47], and Cockx et al. [48]. The MT process in CO_2 absorption into NaOH has been numerically simulated. In addition, the MT from rising spherical bubbles was simulated based on CFD. This particular field of BC research will be developing very fast over the next decade due to the enhanced capabilities of the numerical simulations.

6. Methods for Estimation of the Gas–Liquid Interfacial Area

The gas–liquid interfacial area is an important design and MT variable. Over the past five decades, numerous techniques have been used to measure this key MT parameter in gas–liquid dispersions. There are two main methods to measure the gas–liquid interfacial area: physical and chemical. The physical methods are based on the measurement of the Sauter-mean bubble diameter and the overall gas holdup. When a chemical method is used to determine the gas–liquid interfacial area, a suitable chemical reaction must be applied. Schumpe and Deckwer [49] have recommended the chemical reactions of sulfite oxidation and CO_2 absorption in alkali. Other authors have proposed reactions in organic solvents. The interfacial area determined from the physical and chemical methods may differ more than 100%. In the case of homogeneous bubbly flow, Schumpe and Deckwer [50] have found that the interfacial area determined by the sulfite oxidation method should be multiplied by a factor of 1.35 in order to match the photographically determined interfacial area. In the case of a churn-turbulent regime, the difference is even larger. The other chemical methods used are as follows: aeration with air of 0.072 M $Na_2S_2O_4$ or 0.0975 M

NaOH, aeration with CO_2 of 2 M MEA or water, aeration with CO_2 of 0.95 M NaOH, aeration with CO_2 of 2 M DEA or diethylene glycol, aeration with isobutene of H_2SO_4 (50 wt %) or 2 M t-butanol, aeration with oxygen of 0.392 M CuCl or 5 M HCl, and finally aeration with air of 0.8 M Na_2SO_3. These methods are summarized in Shah et al. [51]. The authors recommend a chemical method (such as sulfite oxidation) with low conversion be used for the measurement of the interfacial area.

Akita and Yoshida [52] have developed the following correlation for the interfacial area per unit dispersion volume:

$$aD_C = \frac{1}{3}\left(\frac{gD_C^2\rho_L}{\sigma_L}\right)^{0.5}\left(\frac{gD_C^2}{\nu_L^2}\right)^{0.1}\varepsilon_g^{1.13} \quad (8)$$

Leonard et al. [26] argue that the interfacial area increases as the operating pressure elevates. The bubble size shrinks, and this leads to the increase of the gas holdup, which ultimately increases the interfacial area. The authors have concluded that the increase of k_La is mainly due to the increase of the interfacial area. The latter also increases with the temperature, which leads to the same effect of temperature on k_La. The increase of viscosity leads to lower interfacial areas and thus lower k_La values. The addition of surface active compounds results in an increase of the k_La values [26].

It is noteworthy that the classical definition (in case of rigid spherical bubbles) of the interfacial area is $6\varepsilon_g$ divided by the Sauter-mean bubble diameter d_S. When this ratio is further divided by the liquid holdup $(1-\varepsilon_g)$, then the interfacial area per unit liquid volume is defined (Lemoine et al. [36]).

7. Conclusions

In this review work, the different measurement techniques and latest approaches for the prediction of the mass transfer coefficients k_La have been discussed. It has been clearly underlined that a complete mixing assumption is not enough for k_La estimation in tall BCs, and a system of two partial differential equations should be solved. Both the liquid and gas axial dispersion coefficients should be considered for the accurate estimation of the k_La coefficients. The most reliable empirical correlations for prediction of the k_La coefficients have been summarized. Their ranges for applicability have been specified. In addition, it has been explained that Higbie's penetration theory should be applied together with a correction factor in the case of non-spherical bubbles. The different correction factors have been presented. The standard definition of the gas–liquid contact time and the one based on local isotropic turbulence theory have been discussed. Finally, the various chemical methods for the determination of the gas–liquid interfacial area have been summarized. Additionally, the main correlation for the prediction of the gas–liquid interfacial area has been reported. The effects of pressure, temperature, and viscosity on the interfacial area and k_La have been discussed.

This review work will help researchers to select the best correlation for estimation of the k_La coefficients under their specific operating conditions. If the researchers need to select an accurate method for k_La measurements, then the most advanced experimental techniques have also been summarized.

Funding: This research received no external funding.

Data Availability Statement: No new experimental data were created.

Conflicts of Interest: The author declares no conflicts of interest.

Abbreviations

Abbreviations		
ADM	axial dispersion model	
BC	bubble column	
CFD	computational fluid dynamics	
DO	dissolved oxygen	
ID	inner diameter	
LIF	laser-induced fluorescence	
MT	mass transfer	
Nomenclature		
a	gas–liquid interfacial area	m^{-1}
d_B	bubble diameter	m
d_S	Sauter-mean bubble diameter	m
D_C	column diameter	m
D_L	molecular diffusivity	m^2/s
f	factor for ionic strength	-
f_c	correction factor	-
G	characteristic of the gas sparger	-
g	acceleration due to gravity	m/s^2
k_L	liquid-phase MT coefficient	m/s
k_La	volumetric liquid-phase MT coefficient	s^{-1}
T	temperature	K
U_g	superficial gas velocity	m/s
Dimensionless numbers		
Bo	Bond number	-
Eo	Eötvös number	-
Fr	Froude number	-
Ga	Galilei number	-
Sc	Schmidt number	-
Sh	Sherwood number	-
Greek letters		
ε_g	gas holdup	-
μ_G	gas viscosity	Pa s
μ_L	liquid viscosity	Pa s
ν	kinematic viscosity	m^2/s
ρ_G	gas density	kg/m^3
ρ_L	liquid density	kg/m^3
σ_L	surface tension	N/m
η	length scale of micro eddies	m
υ	velocity scale of micro eddies	m
$\in$	energy dissipation rate	m^2/s^3

References

1. Deckwer, W.-D.; Adler, I.; Zaidi, A. A comprehensive study on CO_2-interphase mass transfer in vertical concurrent and countercurrent gas-liquid flow. *Can. J. Chem. Eng.* **1978**, *56*, 43–55. [CrossRef]
2. Deckwer, W.-D.; Schumpe, A. Improved tools for bubble column reactor design and scale-up. *Chem. Eng. Sci.* **1993**, *48*, 889–911. [CrossRef]
3. Zahradnik, J.; Kastanek, F.; Kratochvil, J. Hydrodynamics and mass transfer in uniformly aerated bubble column reactors. *Collect. Czechoslov. Chem. Commun.* **1982**, *47*, 262–279. [CrossRef]
4. George, D.L.; Shollenberger, K.L.; Torczynski, J.R. Sparger effects on gas volume fraction distributions in vertical bubble-column flows as measured by gamma-densitometry tomography. *FED Am. Soc. Mech. Eng.* **2000**, *251*, 1487–1494.

5. Xue, J.; Al-Dahhan, M.; Dudukovic, M.P.; Mudde, R.F. Bubble dynamics measurements using four-point optical probe. *Can. J. Chem. Eng.* **2003**, *81*, 375–381. [CrossRef]
6. Deckwer, W.-D.; Hallensleben, J.; Popovic, M. Exclusion of gas sparger influence on mass transfer in bubble columns. *Can. J. Chem. Eng.* **1980**, *58*, 190–197. [CrossRef]
7. Deckwer, W.-D. Non-isobaric bubble columns with variable gas velocity. *Chem. Eng. Sci.* **1976**, *31*, 309–317. [CrossRef]
8. Nedeltchev, S.; Ookawara, S.; Ogawa, K. Quality of mixedness profiles based on spatial distribution of local mass transfer coefficients in a bubble column. *Can. J. Chem. Eng.* **2003**, *81*, 597–603. [CrossRef]
9. Martin, M.; Galan, M.; Cerro, R.L.; Montes, F.J. Shape oscillating bubbles-hydrodynamics and mass transfer-a review. *Bubble Sci. Eng. Technol.* **2011**, *3*, 48–63. [CrossRef]
10. Xu, X.; Kordorwu, V.; Li, Z.; Liu, F. Experimental study on the dynamics and mass transfer of CO_2 bubbles rising in viscoelastic fluids. *Int. J. Multiph. Flow* **2021**, *135*, 103539. [CrossRef]
11. Miguet, J.; Scheid, B.; Dorbolo, S. Antibubble column: A mean to measure and enhance liquid-gas mass transfer through surfactant-laden interfaces. *Chem. Eng. J.* **2024**, *498*, 153276. [CrossRef]
12. Hu, G.; Cui, K.; Jin, S.; Liu, K. Effect of surfactant on dynamics and gas-liquid mass transfer for single carbon dioxide bubbles. *J. Clean. Prod.* **2024**, *453*, 142148. [CrossRef]
13. Dong, X.; Liu, Z.; Liu, F.; Li, Z.; Wei, W.; Wang, X.; Xu, X. Effect of liquid phase rheology and gas-liquid interface property on mass transfer characteristics in bubble columns. *Chem. Eng. Res. Des.* **2019**, *142*, 25–33. [CrossRef]
14. Hebrard, G.; Zeng, J.; Loubiere, K. Effect of surfactants on liquid side mass transfer coefficients: A new insight. *Chem. Eng. J.* **2009**, *148*, 132–138. [CrossRef]
15. Terasaka, K.; Hullmann, D.; Schumpe, A. Mass transfer in bubble columns studied with an oxygen optode. *Chem. Eng. Sci.* **1998**, *53*, 3181–3184. [CrossRef]
16. Han, L.; Al-Dahhan, M.H. Gas-liquid mass transfer in a high pressure bubble column reactor with different sparger designs. *Chem. Eng. Sci.* **2007**, *62*, 131–139. [CrossRef]
17. Huang, J.; Saito, T. Influence of bubble-surface contamination on instantaneous mass transfer. *Chem. Eng. Technol.* **2015**, *38*, 1947–1954. [CrossRef]
18. Valiorgue, P.; Souzy, N.; El Hajem, M.; Ben Hadid, H.; Simoëns, S. Concentration measurement in the wake of a free rising bubble using planar laser-induced fluorescence (PLIF) with a calibration taking into account fluorescence extinction variations. *Exp. Fluids* **2013**, *54*, 1501. [CrossRef]
19. Lin, T.-J.; Tsuchiya, K.; Fan, L.-S. Bubble flow characteristics in bubble columns at elevated pressure and temperature. *AIChE J.* **1998**, *44*, 545–560. [CrossRef]
20. Luo, X.; Lee, D.J.; Lau, R.; Yang, G.; Fan, L.-S. Maximum stable bubble size and gas holdup in high-pressure slurry bubble columns. *AIChE J.* **1999**, *45*, 655–680. [CrossRef]
21. Higbie, R. The rate of absorption of a pure gas into a still liquid during short periods of exposure. *Trans. Am. Inst. Chem. Eng.* **1935**, *31*, 365–389.
22. Miller, D.N. Scale-up of agitated vessels gas-liquid mass transfer. *AIChE J.* **1974**, *20*, 445–453. [CrossRef]
23. Nedeltchev, S.; Jordan, U.; Schumpe, A. Correction of the penetration theory based on mass-transfer data from bubble columns operated in the homogeneous regime under high pressure. *Chem. Eng. Sci.* **2007**, *62*, 6263–6273. [CrossRef]
24. Nock, W.J.; Heaven, S.; Banks, C.J. Mass transfer and gas-liquid interface properties of single CO_2 bubbles rising in tap water. *Chem. Eng. Sci.* **2016**, *140*, 171–178. [CrossRef]
25. Olsen, J.E.; Dunnebier, D.; Davies, E.; Skjetne, P.; Marud, J. Mass transfer between bubbles and seawater. *Chem. Eng. Sci.* **2017**, *161*, 308–315. [CrossRef]
26. Leonard, C.; Ferrasse, J.-H.; Boutin, O.; Lefevre, S.; Viand, A. Bubble column reactors for high pressures and high temperatures operation. *Chem. Eng. Res. Des.* **2015**, *100*, 391–421. [CrossRef]
27. Letzel, H.M.; Schouten, J.C.; Krishna, R.; Van den Bleek, C.M. Gas holdup and mass transfer in bubble column reactors operated at elevated pressure. *Chem. Eng. Sci.* **1999**, *54*, 2237–2246. [CrossRef]
28. Maalej, S.; Benadda, B.; Otterbein, M. Influence of pressure on the hydrodynamics and mass transfer parameters of an agitated bubble column reactor. *Chem. Eng. Technol.* **2001**, *24*, 77–84. [CrossRef]
29. Jordan, U.; Schumpe, A. The gas density effect on mass transfer in bubble columns with organic liquids. *Chem. Eng. Sci.* **2001**, *56*, 6267–6272. [CrossRef]
30. Jordan, U.; Terasaka, K.; Kundu, G.; Schumpe, A. Mass transfer in high-pressure bubble columns with organic liquids. *Chem. Eng. Technol.* **2002**, *25*, 262–265. [CrossRef]
31. Lau, R.; Peng, W.; Velazquez-Vargas, L.G.; Yang, G.Q.; Fan, L.-S. Gas-liquid mass transfer in high-pressure bubble columns. *Ind. Eng. Chem. Res.* **2004**, *43*, 1302–1311. [CrossRef]
32. Gopal, J.S.; Sharma, M.M. Mass transfer characteristics of low H/D bubble columns. *Can. J. Chem. Eng.* **1983**, *61*, 517–526. [CrossRef]

33. Akita, K.; Yoshida, F. Gas hold-up and volumetric mass transfer coefficients in bubble columns. *Ind. Eng. Chem. Process Des. Dev.* **1973**, *12*, 76–80. [CrossRef]
34. Hikita, H.; Asai, S.; Tanigawa, K.; Segawa, K.; Kitao, K. The volumetric mass transfer coefficient in bubble columns. *Chem. Eng. J.* **1981**, *22*, 61–67. [CrossRef]
35. Öztürk, S.S.; Schumpe, A.; Deckwer, W.-D. Organic liquids in a bubble column: Hold-ups and mass transfer coefficients. *AIChE J.* **1987**, *33*, 1473–1480. [CrossRef]
36. Lemoine, R.; Behkish, A.; Sehabiague, L.; Heintz, Y.J.; Oukaci, R.; Morsi, B.I. An algorithm for predicting the hydrodynamic and mass transfer parameters in bubble column and slurry bubble column reactors. *Fuel Process. Technol.* **2008**, *89*, 322–343. [CrossRef]
37. Wellek, R.M.; Agrawal, A.K.; Skelland, A.H.P. Shape of liquid drops moving in liquid media. *AIChE J.* **1966**, *12*, 854–862. [CrossRef]
38. Calderbank, P.H. Gas absorption from bubbles. *Chem. Eng.* **1967**, *45*, CE209–CE233.
39. Deckwer, W.-D. On the mechanism of heat transfer in bubble column reactors. *Chem. Eng. Sci.* **1980**, *35*, 1341–1346. [CrossRef]
40. Li, C.; Cui, Y.; Shi, X.; Gao, J.; Lan, X. CFD simulation of mass transfer in bubble columns: Detailed study of mass transfer models. *Chem. Eng. Sci.* **2022**, *264*, 118173. [CrossRef]
41. Chen, J.; Brooks, C.S. Experiments and CFD simulation of mass transfer and hydrodynamics in a cylindrical bubble column. *Chem. Eng. Sci.* **2021**, *234*, 116435. [CrossRef]
42. Hissanaga, A.M.; Padoin, N.; Paladino, E.E. Mass transfer modeling and simulation of a transient homogeneous bubbly flow in a bubble column. *Chem. Eng. Sci.* **2020**, *218*, 115531. [CrossRef]
43. Liu, J.; Zhou, P.; Liu, L.; Chen, S.; Song, Y.; Yan, H. CFD modeling of reactive absorption of CO_2 in aqueous NaOH in a rectangular bubble column: Comparison of mass transfer and enhancement factor model. *Chem. Eng. Sci.* **2021**, *230*, 116218. [CrossRef]
44. Rzehak, R.; Krepper, E. Euler-Euler simulation of mass-transfer in bubbly flows. *Chem. Eng. Sci.* **2016**, *155*, 459–468. [CrossRef]
45. Jain, D.; Kuipers, J.A.M.; Deen, N.G. Numerical modeling of carbon dioxide chemisorption in sodium hydroxide solution in a micro-structured bubble column. *Chem. Eng. Sci.* **2015**, *137*, 685–696. [CrossRef]
46. Krauß, M.; Rzehak, R. Reactive absorption of CO_2 in NaOH: An Euler-Euler simulation study. *Chem. Eng. Sci.* **2018**, *181*, 199–214. [CrossRef]
47. Jia, H.W.; Zhang, P. Mass transfer of a rising spherical bubble in the contaminated solution with chemical reaction and volume change. *Int. J. Heat Mass Transf.* **2017**, *110*, 43–57. [CrossRef]
48. Cockx, A.; Do-Quang, Z.; Audic, J.M.; Liné, A.; Roustan, M. Global and local mass transfer coefficients in waste water treatment process by computational fluid dynamics. *Chem. Eng. Process. Process Intensif.* **2001**, *40*, 187–194. [CrossRef]
49. Schumpe, A.; Deckwer, W.-D. Analysis of chemical methods for determination of interfacial areas in gas-in-liquid dispersions with non-uniform bubble sizes. *Chem. Eng. Sci.* **1980**, *35*, 2221–2234. [CrossRef]
50. Schumpe, A.; Deckwer, W.-D. Vergleich der fotographischen und der sulfit-oxidation-methode zur phasengrenzflächen-bestimmung in blasensäulen. *Chem. Ing. Tech.* **1980**, *52*, 468–469. [CrossRef]
51. Shah, Y.T.; Kelkar, B.G.; Godbole, S.P.; Deckwer, W.-D. Design parameters estimations for bubble column reactors. *AIChE J.* **1982**, *28*, 353–379. [CrossRef]
52. Akita, K.; Yoshida, F. Bubble size, interfacial area and liquid-phase mass transfer coefficients in bubble columns. *Ind. Eng. Chem. Proc. Des. Dev.* **1974**, *13*, 84–91. [CrossRef]

Disclaimer/Publisher's Note: The statements, opinions and data contained in all publications are solely those of the individual author(s) and contributor(s) and not of MDPI and/or the editor(s). MDPI and/or the editor(s) disclaim responsibility for any injury to people or property resulting from any ideas, methods, instructions or products referred to in the content.